JFM RAPIDS
journals.cambridge.org/rapids

Drag reduction on drop during impact on multiscale superhydrophobic surfaces

Grégoire Martouzet[1], Choongyeop Lee[2], Christophe Pirat[1], Christophe Ybert[1] and Anne-Laure Biance[1],†

[1]Université de Lyon, Université Claude Bernard Lyon 1, CNRS, Institut Lumière Matière, F-69622, VILLEURBANNE, France
[2]Department of Mechanical Engineering, Kyung Hee University, Yongin 17104, Republic of Korea

Liquid drop impact dynamics depends on the liquid–substrate interaction. In particular, when liquid–solid friction is decreased, the spreading of the impacting drop lasts longer. We characterise this effect by using two types of superhydrophobic surfaces, with similar wetting properties but different friction coefficients. It is found that, for large enough impact velocities, a reduced friction delays the buildup of a viscous boundary layer, and leads to an increase of the time required to reach the maximal radius of the impacting drop. An asymptotic analysis is carried out to quantify this effect, and agrees well with the experimental findings. Interestingly, this novel description complements the general picture of drop impact on solid surfaces, and more generally addresses the issue of drag reduction in the presence of slippage for non-stationary flows.

Key words: drops, drag reduction, capillary flows

1. Introduction

Despite being microscopic in nature, the liquid–solid interface can have a strong influence on various macroscale dynamics, such as liquid drop impact on solid surfaces (Yarin 2006), solid-body impact into a liquid pool (Duez *et al.* 2007) and inertial separation between liquid flow and solid (Duez *et al.* 2010). Drop impact on a solid surface has been of particular interest for understanding the complex physical phenomena involved, as well as for its consequences in many industrial processes (Josserand & Thoroddsen 2016). Despite its huge interest, the effect of surface wettability on droplet impact dynamics remains debated. On the one hand, experiments show its pronounced role on spreading (Bayer & Megaridis 2006; Vadillo *et al.* 2009; Liu *et al.* 2014) or bouncing (Richard & Quere 2000) at

† Email address for correspondence: anne-laure.biance@univ-lyon1.fr

low impact velocity, whereas others show no influence at larger impact velocities (Clanet *et al.* 2004; Tsai *et al.* 2011). Local characterisation even points to the crucial effect of a trapped air film during impact (de Ruiter *et al.* 2015). On the other hand, a large number of theoretical, numerical and experimental studies have evidenced that surface friction can play an important role during drop impact at large impact velocity, mainly by considering the two limiting cases of frictionless impact (Clanet *et al.* 2004; Tsai *et al.* 2009; Lastakowski *et al.* 2014) and fully frictional impact with a zero velocity condition at the solid substrate (Roisman 2009; Roisman, Berberovic & Tropea 2009; Eggers *et al.* 2010; Schroll *et al.* 2010; Lagubeau *et al.* 2012). In the latter case, drop spreading after impact is governed by the buildup of a viscous boundary layer in the vicinity of the substrate. The case of partial friction, however, has hardly been explored.

With the development of micro- and nanofabrication techniques, it is possible to engineer surfaces with well-controlled topography. Particularly, hydrophobic surfaces with micro- or nanoscale features – so-called superhydrophobic (SHPo) surfaces – are found to promote unique liquid dynamic characteristics due to the reduced liquid–solid contact (Callies & Quéré 2005). For example, previously unseen phenomena such as crystallographic splashing (Reyssat *et al.* 2010; Tsai *et al.* 2011), pancake bouncing (Liu *et al.* 2014) and reduced contact time (Bird *et al.* 2013) were observed upon impact on such surfaces. On SHPo surfaces, the presence of a stress-free liquid–gas interface not only affects the wetting properties of the droplet but also results in a frictional drag reduction, which is commonly quantified using the effective slip length denoted b, defined as the ratio of slip velocity to the shear rate at the wall (Choi & Kim 2006; Joseph *et al.* 2006; Ybert *et al.* 2007; Rothstein 2010). This effect has been ignored for impacts of simple fluid drops, as it has been observed to have no consequences on droplet spreading (Clanet *et al.* 2004; Tsai *et al.* 2011), although a giant drag reduction has been observed with complex fluids (Luu & Forterre 2013). Determining how the boundary layer – and the overall impact dynamics – is affected by an intermediate friction is the goal of this study. We focus on a regime at high impact velocities, where the effect of friction on the substrate, quantified by the so-called slip length, is relevant for drop spreading dynamics.

One of the main concerns in conducting quantitative experimental studies on an SHPo surface is that it can sustain a low frictional Cassie–Baxter state as long as the drop interacts with the top region of surface structures without intruding into them (Lee, Choi & Kim 2008). However, during drop impact, the dynamic pressure in the liquid drop might overcome the resistance upon imbibition provided by surface tension, leading to the so-called Cassie-to-Wenzel transition (Bartolo *et al.* 2006; Reyssat *et al.* 2006). It was proposed that the impalement during impact might be avoided by using SHPo surface with nanometric features (Deng *et al.* 2009; Tsai *et al.* 2009), but it would compromise the slip length, as the slip length is proportional to the structural pitch of surface features. This problem can be addressed by employing multiscale superhydrophobic surfaces (Lee & Kim 2011), where microscale features ensure a large slip length, while nanoscale features prevent the detrimental Cassie-to-Wenzel transition.

2. Experiments

We designed two types of multiscale superhydrophobic surfaces (figure 1*a,b* and appendix A), denoted B and C, resulting in both cases in similar large static contact angles, but in different friction characteristics and so different slip lengths for water (table 1). A bare smooth silicon wafer was used as a reference (surface A).
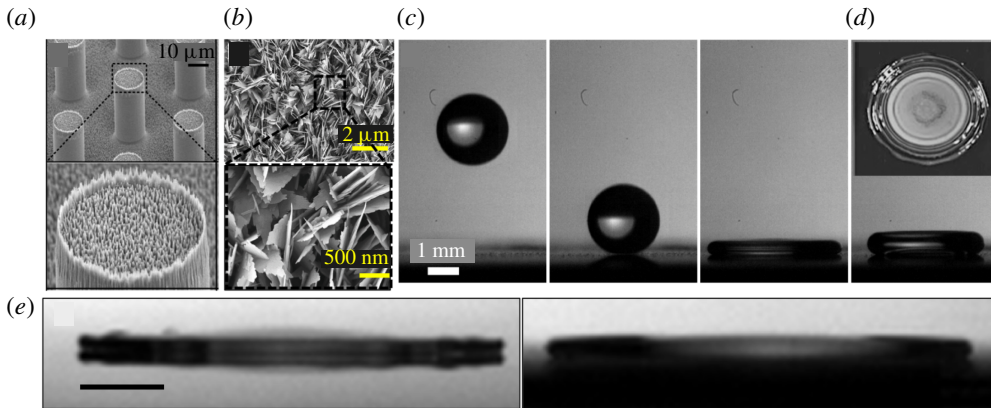
FIGURE 1. Scanning electron microscopy images of (*a*) the textured SHPo surfaces B and (*b*) the disordered SHPo surface C. (*c*) Snapshot of an 80 % mixture of water and glycerol drop impact on surface B ($U = 1.5$ m s^{-1}, time interval 2 ms). (*d*) Top view of a water droplet impact on surface B ($U = 1.5$ m s^{-1}). (*e*) Snapshots of the impact at maximal spreading for impact on surfaces A (left) and B (right); scale bar corresponds to 1 mm ($U = 2.6$ m s^{-1}, $\eta = 21$ cS).

Name	Type	Contact angle (deg.)	Slip length b (µm)	
A	Smooth	$\leqslant 30$	0	
B	Multiscale ordered	$\geqslant 160$	45 ± 5	Lee & Kim (2011)
C	Multiscale disordered	$\geqslant 160$	8 ± 1	

TABLE 1. The three types of surface used and their characteristics.

Drop impact is captured from the side with a high-speed camera (Photron SA-4) at up to 30 000 frames per second (figure 1*c*). The liquids used are mixtures of ultra-pure water and glycerol, with a kinematic viscosity ν ranging from 1 cS (pure water) to 630 cS (pure glycerol). Drops of radius $R \approx 1$ mm are used, with an impact velocity $0.1 < U < 3.5$ m s^{-1}. We introduce as relevant non-dimensional numbers the Weber number $We = \rho R U^2 / \gamma$, which gives the relative importance of inertia compared to surface tension, and the Reynolds number, defined here as $Re = UR/\nu$. Accordingly, We varies between 40 and 1000, and Re between 8 and 11 000. The time $t = \tau$ to reach the maximum spreading radius ($t = 0$ when the drop reaches the substrate) is a relevant parameter to probe the dynamics. The U, R and τ values were detected automatically via image analysis using Python (appendix B). For each set of parameters, three experiments are recorded and τ is averaged.

To confirm that multiscale surfaces ensure robustness towards the Cassie-to-Wenzel transition, a top view image of an impact on SHPo surface B is reported in figure 1(*d*). One can observe that the region where the transition might have occurred, characterised by small dark dots on the picture, is very limited. More interestingly, dynamical wetting properties seem to be very similar in the three cases considered. In figures 1(*c*) and 1(*e*) left and right, corresponding to spreading on surfaces C, A and B, respectively, a dynamic contact angle can be measured and is approximately
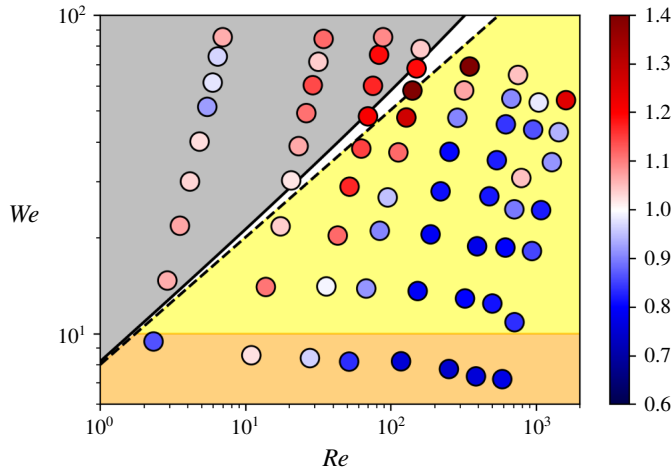
FIGURE 2. Schematic of the drop impact regimes in the *We–Re* phase diagram. Grey, yellow and orange areas correspond, respectively, to the viscous, capillary and inertial regimes (see text). In the case of total friction, the limit between the capillary regime and the viscous regime is determined by the dashed line ($We = 8Re^{2/5}$). In the case of partial friction, the capillary regime is extended towards the grey region until the solid line following $We = 8Re^{2/5}(1 + 0.024Re^{2/5})$, corresponding to $b = 59$ µm. Data points correspond to experiments performed on smooth (A) and rough superhydrophobic surface (B). Colour scales correspond to the value of $\tau(\text{SHPo})/\tau(\text{smooth})$.

$140° \pm 10°$ in both cases, so fully in a hydrophobic regime. We can notice that, in our range of impact parameters, lamella lift-off is never observed.

3. Analysis: scaling laws

The different regimes of drop impact are summarised in figure 2 in the *Re–We* phase diagram. In the frictionless case, two regimes can be identified, depending on *We* values. At low *We*, the inertial time scale to reach the pressure-gradient-free regime ($\tau_i \sim R/U$) is larger than the time scale of capillary recoil ($\tau_c \sim \sqrt{\rho R^3/\gamma}$) and a pancake regime is observed as described in Clanet *et al.* (2004), defined by the orange zone of figure 2. At larger *We*, the rim dynamic limits the drop spreading and $\tau \sim \tau_c = \tau_i We^{1/2}$ (Eggers *et al.* 2010; Lastakowski *et al.* 2014), whatever the impact velocity (Biance, Pirat & Ybert 2011). This regime is defined by the yellow region in figure 2. We limit our study here to $We > 40$, avoiding pancake regimes and coupling between intrusion time scale and spreading (Liu *et al.* 2014).

When friction comes into play, a viscous boundary layer builds up from the substrate. It has been demonstrated numerically (Josserand *et al.* 2005; Eggers *et al.* 2010) and experimentally (Roisman *et al.* 2009; Lagubeau *et al.* 2012; Lastakowski *et al.* 2014) that the spreading is stopped when the viscous boundary layer meets the upper interface of the thinning lamella. Since pressure-free drop thinning follows $h_t \sim R^3/U^2t^2$ (Lastakowski *et al.* 2014), whereas viscous boundary layer development follows $h_{BL} \sim \sqrt{\nu t}$, the spreading dynamics is stopped for a critical lamella thickness satisfying

$$\frac{R^3}{U^2 \tau_v^2} \simeq \sqrt{\nu \tau_v}, \tag{3.1}$$

thus at a viscous time $\tau_v \sim \tau_i Re^{1/5}$. From the comparison of τ_v with τ_c, the viscous regime is dominant over the capillary regime if $We \gtrsim Re^{2/5}$ (Lagubeau *et al.* 2012). This corresponds to the grey region of figure 2.

We now consider the case of a slippery surface. Introducing the slip length b, the no-slip boundary condition is changed to $bu_z = u|_{z=0}$, where u is the fluid velocity tangential to the surface and the subscript z denotes partial differentiation with respect to z. From the unsteady one-dimensional momentum diffusion equation $\partial_t u = \nu \partial_{zz} u$, it can be shown that a self-similar solution for u can be approximated by $u(z, t, b) \simeq U_f(z + b)/\sqrt{\pi \nu t}$ in the vicinity of the surface ($z \sim b$), where U_f is the fluid velocity far from it (appendix C). Asymptotically, the effect of slippage is to shift by $\sim b$ the viscous boundary layer towards the surface, and τ_s, the value of τ in the slippery case, is thus given by

$$\frac{R^3}{U^2 \tau_s^2} \simeq \sqrt{\nu \tau_s} - b. \tag{3.2}$$

Assuming that the slippage has a weak influence on the dynamics, a perturbation of the viscous case readily leads to

$$\tau_s \simeq \tau_v(1 + 2\alpha), \quad \text{with } \alpha = \frac{b}{5\sqrt{\nu \tau_v}} = \frac{b}{5R} Re^{2/5}. \tag{3.3}$$

Comparing τ_s with τ_c, a new critical transition line can be defined in the *Re–We* phase space when slippage effects appear. The result is that the critical domain for which the capillary-driven regime is observed is extended in the viscous regime, and is given by $We \sim Re^{2/5}(1 + 4\alpha)$. This is shown in figure 2, where the classical boundary (no-slip) between capillary and viscous regimes is presented by a dotted line, while the new boundary in the presence of a slip length b appears as a solid line. We focus then on a new regime that should be caused by a slip-delayed viscous boundary layer development.

4. Discussion

We now discuss our experimental results concerning the spreading time reported in figure 3. Deviations between the two cases (impact on smooth and SHPo substrates) are observed whatever the Reynolds number. When the spreading time is larger than the capillary time τ_c, indicated in figure 3 by an orange band, spreading on an SHPo surface is shorter than on a smooth substrate, a surprising behaviour but one that is not in our region of interest. On the contrary, when the spreading time is shorter than the capillary time τ_c, the spreading time observed for impact on smooth surfaces A is always shorter than the one on slippery SHPo surfaces B. Even though significant, this increase could be attributed to rim shape or contact angle differences in both cases. To disentangle the effects of wetting and slippage, we performed similar experiments on surface C, which remains superhydrophobic but with a larger friction coefficient.

We then report in figure 4 the ratio of the spreading time on SHPo surfaces (B or C) to that on smooth substrate (A) $\tau(\text{SPHo})/\tau(\text{smooth})$ in identical impact conditions as a function of the Reynolds number. Comparing surfaces only differing in their slippage properties allows one to evidence a small yet clear experimental effect, with surface B showing a delayed spreading that increases with Reynolds number.
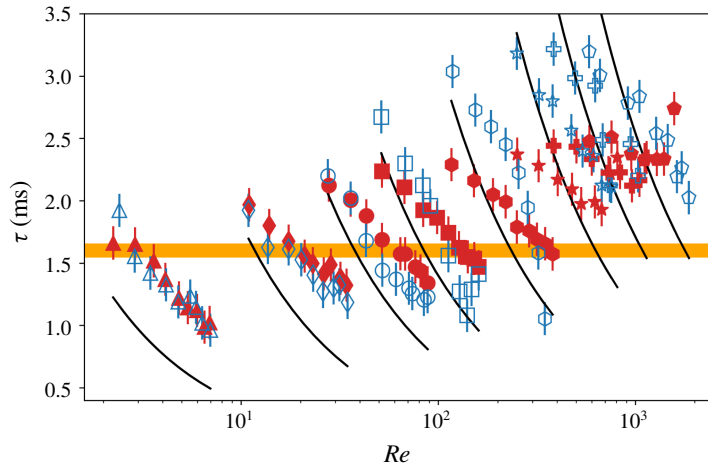
FIGURE 3. Time τ to reach the maximal radius versus the Reynolds number on smooth (A, open symbols) and on SHPo (B, filled symbols) substrates with $\nu = 505$ cS (triangle), $\nu = 103$ cS (diamond), $\nu = 40.5$ cS (circle), $\nu = 21$ cS (square), $\nu = 9.4$ cS (hexagon), $\nu = 4.3$ cS (star), $\nu = 2.8$ cS (cross) and $\nu = 1.9$ cS (pentagon). Solid lines correspond to $\tau = (R/U)Re^{1/5}$ and the horizontal band corresponds to the interval containing $\tau = 0.41\sqrt{\rho R^3/\gamma}$.
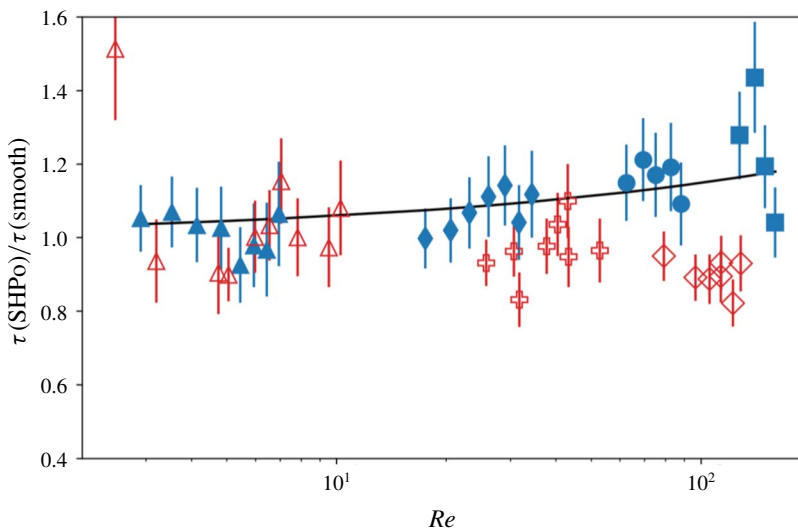

FIGURE 4. Time $\tau(\text{SHPo})$ to reach the maximal radius on slippery surfaces normalised by the time $\tau(\text{smooth})$ to reach the maximal radius on smooth surface. Blue filled symbols, ordered rough surface B; open red symbols, disordered rough surface C. For ordered rough surfaces, viscosities are $\nu = 505$ cS (triangle), $\nu = 103$ cS (diamond), $\nu = 40.5$ cS (circle) and $\nu = 21$ cS (square). For disordered rough surfaces, viscosity used are $\nu \geqslant 250$ cS (triangle), $\nu = 67$ cS (cross) and $\nu = 27$ cS (star). The solid line corresponds to adjustment by (3.3) with $b = 59$ µm.

On the contrary, surface C shows a spreading essentially identical to a classical no-slip wetting surface, with even a slightly shortened spreading, a behaviour we can attribute to either contact-line effects (Laan *et al.* 2014) or fragmentation (Wachters & Westerling 1966). To show a quantitative agreement, a fit of our data with (3.3) is performed, allowing us to define an average slip length b of the order of 59 ± 8 µm. This value is fully consistent with the slip length obtained by torque measurements (40–50 µm) for water on the same surfaces (Lee & Kim 2011). However, considering that our analysis is performed for a two-dimensional stationary flow, that the slip length varies with the liquid viscosity and nature (here water–glycerol mixtures instead of water), the applied pressure (Lee & Kim 2011) (here dynamical pressure during impact), as well as a partial transient impalement on the microstructure, the quantitative comparison should be taken cautiously.

To define more generally the range of parameters for which these effects are relevant, we report experimental observations on the *Re–We* diagram defined in figure 2. The colour bar corresponds to the experimental values of the ratio $\tau(\text{SHPo})/\tau(\text{smooth})$. One can indeed observe an increase of this ratio in the viscous regime. A new frontier between the capillary and slippery regimes can be defined by balancing τ_s and τ_c (figure 2).

5. Conclusion

We propose here a semi-analytical analysis that accounts for drag reduction on viscous impact. A phase diagram is built to better identify the physical parameters for which these effects on the overall dynamics are relevant. It shows the consequences of a weak friction on the spreading dynamics, which can be crucial in many situations. To test it, impacts are performed on two types of multiscale SHPo surfaces, which both resist the Cassie–Baxter-to-Wenzel transition and have similar wetting properties but different friction characteristics. Longer spreading is indeed observed for the lower friction.

Taking into account this effect would be particularly relevant for the design of efficient cooling or anti-icing systems built upon such substrates, where increasing heat transfer through extended contact time and on an extended surface is of crucial interest. On a more fundamental prospect, we propose here an experimental demonstration and a simple analysis of the effect of slippage on the buildup of a viscous boundary layer in a non-stationary flow, a complex mathematical problem (Matthews & Hill 2008; Gie & Kelliher 2012), still investigated recently (Fujioka & Wei 2018).

Declaration of interests

The authors report no conflict of interest.

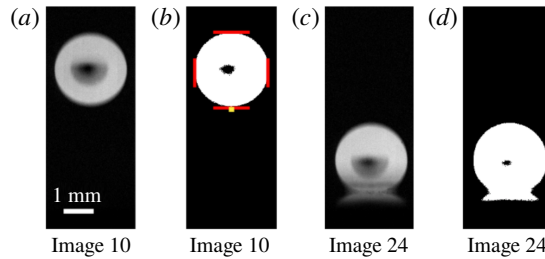| (a) | (b) | (c) | (d) |

1 mm

Image 10   Image 10   Image 24   Image 24

FIGURE 5. Analysed images from a video of a spreading droplet of a 70 % glycerol–water mixture on surface C: (*a*,*c*) images with subtracted background; (*b*,*d*) binary images.

Appendix A. Surface fabrication and characterisation

Surface B is a well-structured surface with multiscale pillars. First, micro-sized cylindrical pillars were obtained using photolithography, followed by deep reactive ion etching on silicon. Pillars are arranged in a square lattice with a fixed structural pitch L (centre-to-centre distance of two adjacent pillars) of 50 µm. The top pillar area fractions $\phi_s = \pi D^2/(4L^2)$, with D the pillar diameter, is set to 0.1. Then, over microscale pillars, nanoscale pillars with a structural pitch of 0.5–1 µm and very sharp tips were generated using a self-masking nanofabrication method known as the black silicon method (Sun *et al.* 2010; Lee & Kim 2011). The surface is made hydrophobic with a few nanometres thick Teflon layer coating. Using torque measurements, the slip length of water on this surface is found to be approximately 35 ± 5 µm.

Surface C is a randomly textured surface made of CuO obtained by oxidation of a copper sample in a mixture of $NaClO_2$, NaOH and Na_3PO_4. It is made hydrophobic by silane vapour deposition. Images of the surface are reported in figure 1. The slip length from water Poiseuille flow rate measurements in a microfluidic channel is found to be 8 ± 1 µm. Note that, even if slip length measurement methods are different for the two surfaces, they both involve a relatively low liquid pressure and a laminar flow condition, and they can be reasonably compared (Lee *et al.* 2016).

Static angles on both surfaces were found to be similar and above 160°. Dynamical contact angles during the spreading are also similar in the three cases of smooth substrate (A) and superhydrophobic surfaces (B and C), larger than 160°.

Appendix B. Spreading time detection and accuracy

Typical snapshots of impact recording are reported in figure 1. The droplet contour and position are determined by subtracting the background and thresholding (figure 5). Results are hardly dependent on the choice of the threshold (1 pixel). The contact time origin is automatically determined by looking at the presence of a bright pixel below the drop. The droplet maximum radius is determined by fitting the evolution of the droplet radius versus time and fitting the curve in the vicinity of the maximum by a second-order polynomial. The maximum of the function and the time to reach this maximum correspond then for each experiment at the spreading radius and spreading time, respectively. Finally, the spreading time uncertainty is 0.17 ms.

Appendix C. Boundary layer development over a surface with a Navier condition

C.1. *Two-dimensional analysis – infinite surface*

We consider the motion of a liquid near a solid infinite plane located at $z = 0$. The liquid and the plate are initially at rest and then the plate is moved at a velocity U_f, in the x direction. We investigate the development of a viscous boundary layer in the z direction taking into account this effect. The momentum diffusion equation locally reads

$$\frac{\partial u_x}{\partial t} = v \frac{\partial^2 u_x}{\partial z^2}, \tag{C 1}$$

where v is the kinematic viscosity of the liquid.

Introducing $\xi = z/\sqrt{vt}$ and the two constants A and B, the solution of (C 1) is

$$u_x(z, t) = A \int_0^{\xi} e^{-y^2/4} \, dy + B. \tag{C 2}$$

Boundary conditions are that: (i) the fluid is at rest far from the surface, ($\lim u_x(x \to +\infty) = 0$); and (ii) in the vicinity of the surface ($z = 0$), the slip condition is defined by slip length b, where $b(\partial u_x/\partial z)|_{z=0} = u_x|_{z=0} - U_f$. Then, the velocity profile reads

$$u_x(z, t) = \frac{U_f}{\dfrac{b}{\sqrt{\pi vt}} + 1} \left(1 - \mathrm{erf}\left(\frac{z}{\sqrt{4vt}} \right) \right), \tag{C 3}$$

where we recover its usual form for $b = 0$. The deviation due to slippage is then

$$\frac{u_x(z, t, b)}{u_x(z, t, 0)} = \frac{1}{\dfrac{b}{\sqrt{\pi vt}} + 1}. \tag{C 4}$$

This term is negligible when $t \geqslant b^2/v$. As the boundary layer develops from the substrate, it reaches the altitude z after a characteristic time z^2/v; the effect of slippage will be important if $b \geqslant z$. We define the effect of slip on the altitude at which viscous friction is felt versus time. Considering that the viscous friction is felt when $u_x(z, t)/U_f = k$, with k between 0 and 1, the time-dependent z at which viscous effects are important reads

$$z(b, t, k) = \sqrt{4vt} \, \mathrm{erf}^{-1}\left(1 - k - \frac{bk}{\sqrt{\pi vt}} \right). \tag{C 5}$$

The effect of slippage can be captured by estimating $z(b, t, k \to 1) - z(0, t, k \to 1)$. When $t \to \infty$, this value is converging to b. The boundary layer is shifted up by a length b.

C.2. *Consequences on droplet dynamics upon impact: time scales*

We consider a drop impacting on a solid substrate. We distinguish here the three cases of drop impact without friction (i.e. Leidenfrost case), with large friction (smooth solid substrate) and with slippage (superhydrophobic substrate). For each regime, we identify the characteristic time to reach the maximal radius, and these times will be compared to identify which regime is predominant as a function of the Weber $We = \rho R^3/\gamma$ and Reynolds $Re = UR/v$ numbers.

C.2.1. *Frictionless case*

In this regime, two cases can be determined depending only on the Weber number. A deceleration phase over a time $\tau_i \sim R/U$ (Clanet *et al.* 2004) is followed by a capillary oscillation over $\tau_c \sim \sqrt{\rho R^3/\gamma}$. If τ_c is smaller than τ_i, only the deceleration is observed and we reach a pancake regime, whereas on the contrary a capillary recoil (Roisman *et al.* 2009; Eggers *et al.* 2010; Lastakowski *et al.* 2014) is observed. The transition is given by $\tau_c = \tau_i$, which implies a critical Weber number We_1. In the following analysis, we assume that We is always above We_1.

C.2.2. *Large friction*

In this case, it has been shown that the development of a boundary layer sets the maximal attained radius, i.e. when the droplet thickness is comparable to this developed boundary layer, the droplet stops spreading and thinning. For We larger than We_1, this criterion reads (Roisman *et al.* 2009; Eggers *et al.* 2010; Lastakowski *et al.* 2014)

$$\frac{R^3}{U^2(\tau_v)^2} \simeq k\sqrt{\nu(\tau_v)} \tag{C6}$$

and then the spreading viscous time scales as $\tau_v \sim \tau_i Re^{1/5}$. This regime is relevant if this time is shorter than τ_c, i.e. $We \gtrsim Re^{2/5}$.

C.2.3. *Slippage*

Following previous asymptotic analysis, the characteristic time τ_s to develop the boundary layer over the distance h satisfies

$$\frac{R^3}{U^2\tau_s^2} \simeq k\sqrt{\nu\tau_s} - b. \tag{C7}$$

Let us now assume that the effect of slippage is small compared to viscous effects. The characteristic viscous slippery time τ_s can then be written as

$$\tau_s = \tau_v + t_s \tag{C8}$$

with $t_s = o(\tau_v)$ the slippage contribution. Equation (C7) can then be developed as

$$-\frac{R^3}{U^2\tau_v^2}\frac{2t_s}{\tau_v} \simeq k\sqrt{\nu\tau_v}\frac{t_s}{2\tau_v} - b, \tag{C9}$$

$$\tau_s \simeq \tau_v\left(1 + \frac{2b}{5R}Re^{2/5}\right). \tag{C10}$$

The capillary region is then extended to $We \lesssim Re^{2/5}(1 + (2b/5R)Re^{2/5})$ (figure 2).

References

BARTOLO, D., EOUAMRIRENE, F., VERNEUIL, E., BUGUIN, A., SILBERZAN, P. & MOULINET, S. 2006 Bouncing or sticky droplets: impalement transitions on superhydrophobic micropatterned surfaces. *Eur. Phys. Lett.* **74**, 299–305.

BAYER, I. S. & MEGARIDIS, C. M. 2006 Contact angle dynamics in droplets impacting on flat surfaces with different wetting characteristics. *J. Fluid Mech.* **558**, 415–449.

BIANCE, A.-L., PIRAT, C. & YBERT, C. 2011 Drop fragmentation due to hole formation during Leidenfrost impact. *Phys. Fluids* **23** (2), 022104.

BIRD, J. C., DHIMAN, R., KWON, H.-M. & VARANASI, K. K. 2013 Reducing the contact time of a bouncing drop. *Nature* **503** (7476), 385–388.

CALLIES, M. & QUÉRÉ, D. 2005 On water repellency. *Soft Matt.* **1** (1), 55–61.

CHOI, C.-H. & KIM, C.-J. 2006 Large slip of aqueous liquid flow over a nanoengineered superhydrophobic surface. *Phys. Rev. Lett.* **96** (6), 066001.

CLANET, C., BEGUIN, C., RICHARD, D. & QUERE, D. 2004 Maximal deformation of an impacting drop. *J. Fluid Mech.* **517**, 199–208.

DENG, T., VARANASI, K. K., HSU, M., BHATE, N., KEIMEL, C., STEIN, J. & BLOHM, M. 2009 Nonwetting of impinging droplets on textured surfaces. *Appl. Phys. Lett.* **94**, 133109.

DUEZ, C., YBERT, C., CLANET, C. & BOCQUET, L. 2007 Making a splash with water repellency. *Nat. Phys.* **3** (3), 180–183.

DUEZ, C., YBERT, C., CLANET, C. & BOCQUET, L. 2010 Wetting controls separation of inertial flows from solid surfaces. *Phys. Rev. Lett.* **104** (8), 084503.

EGGERS, J., FONTELOS, M. A., JOSSERAND, C. & ZALESKI, S. 2010 Drop dynamics after impact on a solid wall: theory and simulations. *Phys. Fluids* **22**, 062101.

FUJIOKA, H. & WEI, H.-H. 2018 Letter: new boundary layer structures due to strong wall slippage. *Phys. Fluids* **30** (12), 121702.

GIE, G.-M. & KELLIHER, J. P. 2012 Boundary layer analysis of the Navier–Stokes equations with generalized navier boundary conditions. *J. Differ. Equ.* **253** (6), 1862–1892.

JOSEPH, P., COTTIN-BIZONNE, C., BENOIT, J.-M., YBERT, C., JOURNET, C., TABELING, P. & BOCQUET, L. 2006 Slippage of water past superhydrophobic carbon nanotube forests in microchannels. *Phys. Rev. Lett.* **97** (15), 156104.

JOSSERAND, C., LEMOYNE, L., TROEGER, R. & ZALESKI, S. 2005 Droplet impact on a dry surface: triggering the splash with a small obstacle. *J. Fluid Mech.* **524**, 47–56.

JOSSERAND, C. & THORODDSEN, S. T. 2016 Drop impact on a solid surface. *Annu. Rev. Fluid Mech.* **48** (1), 365–391.

LAAN, N., DE BRUIN, K. G., BARTOLO, D., JOSSERAND, C. & BONN, D. 2014 Maximum diameter of impacting liquid droplets. *Phys. Rev.* A **2**, 044018.

LAGUBEAU, G., FONTELOS, M. A., JOSSERAND, C., MAUREL, A., PAGNEUX, V. & PETITJEANS, P. 2012 Spreading dynamics of drop impacts. *J. Fluid Mech.* **713**, 50–60.

LASTAKOWSKI, H., BOYER, F., BIANCE, A.-L., PIRAT, C. & YBERT, C. 2014 Bridging local to global dynamics of drop impact onto solid substrates. *J. Fluid Mech.* **747**, 103–118.

LEE, C., CHOI, C.-H. & KIM, C. J. 2008 Structured surfaces for a giant liquid slip. *Phys. Rev. Lett.* **101**, 064501.

LEE, C. & KIM, C.-J. 2011 Influence of surface hierarchy of superhydrophobic surfaces on liquid slip. *Langmuir* **27**, 4243–4248.

LEE, J. B., LAAN, N., DE BRUIN, K. G., SKANTZARIS, G., SHAHIDZADEH, N., DEROME, D., CARMELIET, J. & BONN, D. 2016 Universal rescaling of drop impact on smooth and rough surfaces. *J. Fluid Mech.* **786**, R4.

LIU, Y., MOEVIUS, L., XU, X., QIAN, T., YEOMANS, J. M. & WANG, Z. 2014 Pancake bouncing on superhydrophobic surfaces. *Nat. Phys.* **10** (7), 515–519.

LUU, L.-H. & FORTERRE, Y. 2013 Giant drag reduction in complex fluid drops on rough hydrophobic surfaces. *Phys. Rev. Lett.* **110** (18), 184501.

MATTHEWS, M. T. & HILL, J. M. 2008 A note on the boundary layer equations with linear slip boundary condition. *Appl. Maths Lett.* **21** (8), 810–813.

REYSSAT, M., PEIN, A., MARTY, F., CHEN, Y. & QUERE, D. 2006 Bouncing transitions on microtextured materials. *Eur. Phys. Lett.* **74**, 306–312.

REYSSAT, M., RICHARD, D., CLANET, C. & QUERE, D. 2010 Dynamical superhydrophobicity. *Faraday Discuss.* **146**, 19–33.

RICHARD, D. & QUERE, D. 2000 Bouncing water drops. *Eur. Phys. Lett.* **50**, 769–775.

ROISMAN, I. V. 2009 Inertia dominated drop collisions. II. An analytical solution of the Navier–Stokes equations for a spreading viscous film. *Phys. Fluids* **21** (5), 052104.

ROISMAN, I. V., BERBEROVIC, E. & TROPEA, C. 2009 Inertia dominated drop collisions. I. On the universal flow in the lamella. *Phys. Fluids* **21**, 052103.

ROTHSTEIN, J. P. 2010 Slip on superhydrophobic surfaces. *Annu. Rev. Fluid Mech.* **42**, 89–109.

DE RUITER, J., LAGRAAUW, R., VAN DEN ENDE, D. & MUGELE, F. 2015 Wettability-independent bouncing on flat surfaces mediated by thin air films. *Nat. Phys.* **11** (1), 48–53.

SCHROLL, R. D., JOSSERAND, C., ZALESKI, S. & ZHANG, W. W. 2010 Impact of a viscous liquid drop. *Phys. Rev. Lett.* **104**, 034504.

SUN, G., GAO, T., ZHAO, X. & ZHANG, H. 2010 Fabrication of micro/nano dual-scale structures by improved deep reactive ion etching. *J. Micromech. Microengng* **20** (7), 075028.

TSAI, P., HENDRIX, M. H. W., DIJKSTRA, R. M., SHUI, L. & LOHSE, D. 2011 Microscopic structure influencing macroscopic splash at high Weber number. *Soft Matt.* **7** (24), 11325–11333.

TSAI, P., PACHECO, S., PIRAT, C., LEFFERTS, L. & LOHSE, D. 2009 Drop impact upon micro- and nanostructured superhydrophobic surfaces. *Langmuir* **25**, 12293–12298.

VADILLO, D. C., SOUCEMARIANADIN, A., DELATTRE, C. & ROUX, D. C. D. 2009 Dynamic contact angle effects onto the maximum drop impact spreading on solid surfaces. *Phys. Fluids* **21** (12), 122002.

WACHTERS, L. H. & WESTERLING, N. A. 1966 Heat transfer from a hot wall to impinging water drops in spheroidal state. *Chem. Engng Sci.* **21**, 1047–1056.

YARIN, A. L. 2006 Drop impact dynamics: splashing, spreading, receding, bouncing.... *Annu. Rev. Fluid Mech.* **38**, 159–192.

YBERT, C., BARENTIN, C., COTTIN-BIZONNE, C., JOSEPH, P. & BOCQUET, L. 2007 Achieving large slip with superhydrophobic surfaces: scaling laws for generic geometries. *Phys. Fluids* **19** (12), 123601.